INTERNATIONAL JOURNAL OF HYDROGEN ENERGY XXX (XXXX) XXX

Available online at www.sciencedirect.com

ScienceDirect

journal homepage: www.elsevier.com/locate/he

Visualization, understanding, and mitigation of process-induced-membrane irregularities in gas diffusion electrode-based polymer electrolyte membrane fuel cells

Min Wang [a,1], *Samantha Medina* [b], *Josias Ochoa-Lozano* [a,c], *Scott Mauger* [a], *Svitlana Pylypenko* [a,b], *Michael Ulsh* [a], *Guido Bender* [a,*]

[a] *Chemistry and Nanoscience Center, National Renewable Energy Laboratory, 15013 Denver West Parkway, Golden, CO, 80401, United States*

[b] *Department of Chemistry, Colorado School of Mines, Golden, CO 80401, United States*

[c] *Department of Chemical and Environmental Engineering, University of California, Riverside, Riverside, CA 92521, United States*

HIGHLIGHTS

- Visualized process-induced morphology changes (PIMs) by IR thermography.
- Elucidated structure & formation mechanism of PIMs by cross-sectional SEM.
- Studied impact of fabrication conditions on PIMs and initial performance.
- Fine tuning fabrication conditions mitigates PIMs in MEA.
- PIMs are seed points for AST failure, and shorten MEA lifetime.

GRAPHICAL ABSTRACT

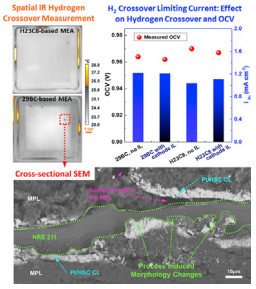

ARTICLE INFO

Article history:
Received 8 October 2020
Received in revised form
20 January 2021
Accepted 26 January 2021
Available online xxx

Keywords:
PEMFC

ABSTRACT

Polymer electrolyte membrane fuel cells (PEMFC) show substantial promise for their application in electric vehicles. For large-scale manufacturing of PEMFCs, roll-to-roll coated gas-diffusion-electrodes (GDE) offer certain advantages over other production pathways. Procedures including hot pressing and coating an ionomer overlayer may be necessary for this manufacturing pathway to enable a suitable catalyst layer/membrane interface. The same procedures may potentially introduce membrane irregularities, especially when thin membranes are used. Limited understanding exists regarding if and to what extent such irregularities impact PEMFC performance and lifetime, and therefore be considered defects.

* *Corresponding author.*
E-mail address: guido.bender@nrel.gov (G. Bender).
[1] Currently at Southern University of Science and Technology, Shenzhen 518055, P.R. China.
https://doi.org/10.1016/j.ijhydene.2021.01.186

MEA
Membrane irregularity
Hot pressing
IR
AST

In this study, NREL's customized fuel cell hardware that enables quasi in-situ infrared (IR) thermography studies was utilized to visualize spatial hydrogen crossover and identify membrane irregularities that originated from the GDE-based MEA fabrication process. The structure of these membrane irregularities was investigated by scanning electron microscopy (SEM) and its impact on initial H_2/air performance was determined. Accelerated stress testing (AST) revealed that these irregularities develop into failure point locations. These results were validated across many MEAs with identified process-induced membrane irregularities. By selecting specific gas diffusion media properties and by fine tuning the MEA hot pressing parameters, the formation of such membrane irregularities was mitigated.

Introduction

Polymer electrolyte membrane fuel cells (PEMFCs) are promising environmentally-friendly energy conversion devices that are applicable to vehicles and other power generation applications [1–9]. To lower cost and facilitate the introduction of PEMFCs to the market, it is necessary to manufacture fuel cell components with high quality at high volume [10]. The National Renewable Energy Laboratory (NREL) fuel cell manufacturing effort conducts R&D that supports the transition from lab-scale fabrication to large-scale manufacturing [11]. In practical manufacturing of fuel cell materials, material irregularities can be introduced which may result in lower performance and early failure [12–15]. NREL has developed a number of quality control methods that identify materials irregularities [16–21]. However, limited research has been done to study the impacts of these irregularities on PEMFC performance and lifetime. Understanding this impact is important, as it is necessary to define the threshold at which an irregularity becomes a defect, i.e. a material variation that impacts membrane electrode assembly (MEA) performance or lifetime. Such thresholds enable the development of quality control standards or tolerances, which define the criteria with which to accept materials with a certain variation, and which may reduce MEA production cost and increase efficiency and yield. These benefits could be all the more significant within the context of fuel cells for medium- and heavy-duty applications, such as long-haul trucks, where the targets for fuel efficiency and stack lifetime – due to the increased impact of fuel costs on the lifecycle cost of the vehicle – are even more stringent than in the case of light-duty vehicles [22,23].

The key component of a PEMFC is the MEA, which consists of gas diffusion media (GDM), catalyst layers and membrane material. There are two common methods to construct MEAs: via catalyst-coated membranes (CCM) or via gas-diffusion electrodes (GDE), for which the catalyst layer is directly applied to the membrane or to the GDM, respectively [24]. CCMs are the preferred fabrication method in most research efforts because they achieve good performance with routine fabrication methods. However, manufacturing CCMs in high volume with roll-to-roll coating systems is challenging due to the swelling that the membrane material experiences when exposed to the solvents in catalyst inks. For this reason, coating the catalyst layer (CL) onto the GDM to create a GDE is potentially more facile for manufacturing [10]. Historically, GDEs were thought to have inferior performance to CCMs due to a high contact resistance at the CL/membrane interface. However, work has been done to enhance the performance of GDE-based MEAs by improving this interface. Lin et al. investigated how hot pressing improved the interface and performance of GDE-based MEAs [25]. Shahgaldi et al. demonstrated that adding an ionomer layer onto GDEs improves their performance [26]. In previous work, our group established that spraying a thin ionomer overlayer (IL) onto a GDEs and subsequently hot pressing it to the membrane results in a good CL/membrane interface and a performance comparable to that of a CCM-based MEA [27]. We further explored the impact of microporous layer (MPL) roughness on the CL/membrane interface and cell performance [28]. All this work focused on improving the CL/membrane interface, enhancing PEMFC performance, and ultimately providing a pathway to use GDEs in the mass production of fuel cells.

In the fabrication of GDE-based MEAs, it is implied that the GDEs will be mated with a membrane in some form of MEA or cell assembly process [24]. During such processes, e.g. hot pressing (HP), it can be envisioned that membrane irregularities such as holes, fissures, and thin spots could be introduced as a result of handling, alignment, and/or compression of the various cell materials, especially when thin membranes are used. Previous studies demonstrated that hot pressing has a large impact on electrochemical surface area [25,29], catalyst layer porosity and structure [30,31], and single cell performance [25,30–33]. These studies demonstrate that HP with different compression force and temperature affect the CL porosity and the CL/membrane contact resistance, aiming to optimize HP conditions based on polarization performance. However, to the best of our knowledge, the impact of hot pressing on membrane quality, open-circuit voltage or gas crossover has not been not investigated.

In this work, NREL's customized fuel cell hardware [13] was utilized to visualize hydrogen crossover in pristine GDE-based MEAs and to identify and localize membrane irregularities introduced by the MEA fabrication processes. The structure of the detected irregularities was investigated by scanning electron microscopy (SEM) imaging of MEA cross sections. The

Please cite this article as: Wang M et al., Visualization, understanding, and mitigation of process-induced-membrane irregularities in gas diffusion electrode-based polymer electrolyte membrane fuel cells, International Journal of Hydrogen Energy, https://doi.org/10.1016/j.ijhydene.2021.01.186

impact of the membrane irregularities on PEMFC performance in air, open-circuit voltage (OCV), and hydrogen crossover were systematically studied. In addition, accelerated stress tests (AST) were conducted on the MEAs to understand if the membrane irregularities lead to the development of failure points and thus impact the lifetime of the device.

Experimental

This section describes experimental specifics with regards to materials, sample preparation and characterization.

Materials

A Pt catalyst supported on high surface area carbon (Pt/HSC) was used for both the anode and the cathode (Tanaka Kikinzoku Kogyo TEC10E50E, 46.2 wt% Pt). Nafion dispersion from Ion Power (D2020, 1000 EW at 20 wt%) and HPLC-grade OmniSolv® n-Propanol (n-PA) from Millipore Sigma were used for electrode fabrication. Nafion® 211 membranes from Ion Power (~25 μm) were used for MEA fabrication.

Two types of GDM were investigated: SGL Carbon Sigracet 29BC and Freudenberg H23C8. Both materials feature MPLs with hydrophobic treatment, but otherwise have different structural architecture. In our recent work, the MPL roughness of GDMs was demonstrated to affect the CL/membrane interfacial properties and in-situ performance [28]. In this work, we employed these same two GDM, which are commonly used fuel cell materials, to investigate the impact of MPL roughness on process-induced membrane irregularities. Scanning electron microscopy (FEI Talos F200X) and micrometer-scale surface roughness measurements (Veeco Dektak 8 Stylus Profilometer, tip radius: 5 μm) were conducted on the MPLs of both GDM to investigate their surface structures. 29BC contains visible cracks in the MPL, as shown in Fig. 1(a), while H23C8 has a generally crack-free MPL surface, as shown in Fig. 1(b). Fig. 1(c) shows MPL roughness data for both GDM, measured by stylus profilometry. The data indicate that the 29BC MPL had a much rougher surface than the H23C8 MPL. The root-mean-square (RMS) surface roughness of the 29BC MPL and H23C8 MPL were 15.9 μm and 3.1 μm, respectively.

Ink preparation and GDE fabrication

To prepare the catalyst ink, Pt/HSC powder was mixed with deionized water, n-propanol, and D2020 Nafion dispersion. A standard NREL ink formulation for Pt/HSC catalyst was used [34,35]: 3.75 mg/mL Pt/HSC, ionomer to carbon ratio (I/C) of 0.9, and water-to-alcohol ratio (in volume) of 1:3. The ink was tip sonicated for 10 s (Branson Sonifier SFX250, 250 W) and then bath sonicated for 20 min in an ice bath (Fisher Scientific FS30, 100 W). An ionomer dispersion for adding an ionomer overlayer to the catalyst layer was prepared by diluting the stock Nafion dispersion in water and n-PA. The water-to-n-PA ratio was the same as that of the catalyst ink. The diluted dispersion was stirred overnight prior to use.

The cathode and anode GDEs were prepared by spray coating the catalyst inks onto the GDM at 80 °C with a pump rate of 0.3 mL/min, using a Sono-Tek ExactaCoat System with a 25 kHz Accumist nozzle. The desired catalyst loading was 0.2 ± 0.01 mg Pt/cm^2 for both cathodes and anodes. The catalyst loading was validated by X-ray fluorescence (Fischerscope XDV-SDD, 50 kV, 50 W X-ray source), and the results were averaged over five locations on the 50 cm^2 electrode. For some but not all samples, an ionomer overlayer with a loading of 0.023 mg Nafion/cm^2 was sprayed onto the cathode GDE using a pump rate of 0.15 mL/min at 80 °C, as described in our recent work [28].

MEA fabrication and cell assembly

Edge protection was applied in our study to avoid edge failure during AST operation. Our previous work describes the fabrication of edge protected CCM-based MEAs in detail [36]. In this work, very similar edge protection was applied to GDE-based MEAs. As shown in Figs. S1 and 1 mil (25.4 μm) polytetrafluoroethylene (PTFE) gaskets were placed between the GDEs and the membrane so that the gasket overlapped the GDEs by 1.85 mm on all four sides, and so that the active area was dimensioned to exactly 50 cm^2. To achieve and maintain good alignment, oversized GDM were added on the top and bottom, then hot pressed between two metal sheets, two pieces of Gylon, and two pieces of Kapton film for 3 min. A range of hot pressing temperatures (110–125 °C) and forces (8–25 kg/cm^2) were applied to study the impact of fabrication conditions on initial MEA quality and PEMFC performance.

The hot pressed MEAs were assembled together with two PTFE gaskets. The selected thickness of the gaskets created 25% compression for 29BC or 18% compression for H23C8 materials based on manufacturer specifications. The calculations assumed a 6% gasket compression at a 40 inch-pounds torque.

IR thermography

For in-situ experiments, a previously introduced custom 50 cm^2 single cell hardware was used [13,15]. This hardware facilitates mapping of the hydrogen crossover in "*IR mode*" in addition to providing a platform for regular cell operation, i.e. "*fuel cell mode*". The latest experimental *IR mode* setup is presented in Fig. S2. In this mode, the cathode side of the hardware is partially disassembled and the cathode exposed to ambient conditions (air and room temperature). The anode side of the hardware remains sealed and keeps the MEA aligned and in position. IR thermography was performed as we described in previous work [6]. Briefly, an IR camera (FLIR A300 Series) is employed to record the thermal signature of the cathode. To switch from *fuel cell mode* to *IR mode*, cell operation was interrupted and the pressures and temperatures of the cell ramped down to ambient conditions. Upon initiating a small flow of hydrogen (20 sccm), any hydrogen that diffused through the MEA experienced an exothermic reaction with the ambient oxygen at the surface of the platinum catalyst. The resulting temperature rise was observed by the IR camera.

Electrochemical measurements

A fuel cell test station was used to break in and condition the cell. This procedure has been previously described in detail

Please cite this article as: Wang M et al., Visualization, understanding, and mitigation of process-induced-membrane irregularities in gas diffusion electrode-based polymer electrolyte membrane fuel cells, International Journal of Hydrogen Energy, https://doi.org/10.1016/j.ijhydene.2021.01.186

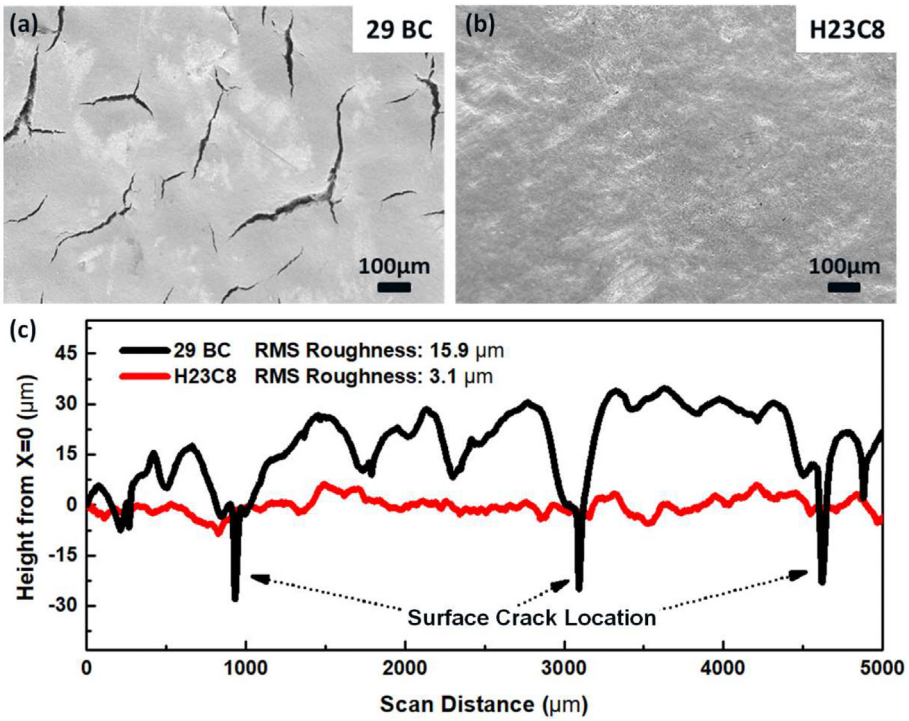

Fig. 1 – Top-down SEM images of the microporous layer of (a) 29BC and (b) H23C8 gas diffusion media; (c) Surface roughness of H23C8 and 29BC microporous layer measured by stylus profilometry.

by Zhang et al. and Kabir et al. [37,38]. H_2/air polarization curves were performed at 80 °C, 150/150 kPa, and 1.5/2 stoichiometric H_2/air flow rates at 100/100% relative humidity (RH) for the anode and cathode, respectively. Data was collected controlling the current and starting from a total cell current density of 1.5 A/cm^2 using the following subsequent steps: 1.0, 0.8, 0.6, 0.4, 0.2, 0.1, and 0.05 A/cm^2, followed by an OCV hold for 10 s.

Hydrogen crossover linear sweep voltammetry (LSV) was measured using a potentiostat (Metrohm Autolab) at a scan rate of 1 mV/s. For the hydrogen crossover measurements, the gas flow was H_2/N_2 for the anode and cathode, respectively. The flow rate was 200/200 sccm, and the cell temperature was 80 °C. The cell was operated at ambient pressure.

Accelerated stress tests have been widely applied to study PEMFC degradation and durability [9,39]. In this work, a combined AST protocol that induces both chemical and mechanical degradation mechanisms of the membrane was used to investigate the failure time and behavior of MEAs with different number of membrane irregularities [13]. The AST was carried out on a fuel cell test station. IR thermography was performed at the beginning (BOT) and the end (EOT) of the AST. Throughout the AST, the cell was held at OCV at 80 °C. Anode/cathode operating conditions were ambient pressures, 500/500 sccm H_2/air gas flow rates, and 30/30 s duty cycle for dry and wet humidification (0/0% and 100/100% RH), respectively. The AST operation was manually stopped when the OCV dropped below 0.9 V. As OCV drops below 0.9V, hydrogen crossover current density (iH_2) increases up to ~6 mA/cm^2 based on theoritical calculations [40], indicating the onset of membrane failure.

Structural characterization

Scanning transmission electron microscope (STEM) images and energy dispersive spectroscopy (EDS) maps were obtained using a FEI Talos F200X electron microscope operating at 200 keV. For analysis of the MEA cross-sections with scanning electron microscopy (SEM), a piece of the MEA was submerged in liquid nitrogen for approximately 20 s, followed by cutting the frozen MEA with a brand-new feather double edge razor blade on a glass slide. The cross-sections were placed on double-sided carbon tape and adhered to a cross-section specimen holder for SEM imaging. Secondary electron images (SEI) and back-scattered electron (BSE) images of the cross-sectional view for MEAs with different diffusion media and fabricated under different conditions were obtained with a JEOL JSM-7000F Field Emission-SEM operating at a 10 kV accelerating voltage and a 10 mm working distance.

Results and discussion

Visualization of membrane irregularities and their impact on performance

Fig. 2 shows results of GDE-based MEAs using 29BC GDM. The samples were fabricated without ionomer overlayer (IL) using different hot pressing (HP) compression forces. As expected from previous work, the initial performance of these samples, which is shown in Fig. 2(a), left much to be desired because of the lack of ionomer overlayer [27,28]. For example, the best

Please cite this article as: Wang M et al., Visualization, understanding, and mitigation of process-induced-membrane irregularities in gas diffusion electrode-based polymer electrolyte membrane fuel cells, International Journal of Hydrogen Energy, https://doi.org/10.1016/j.ijhydene.2021.01.186

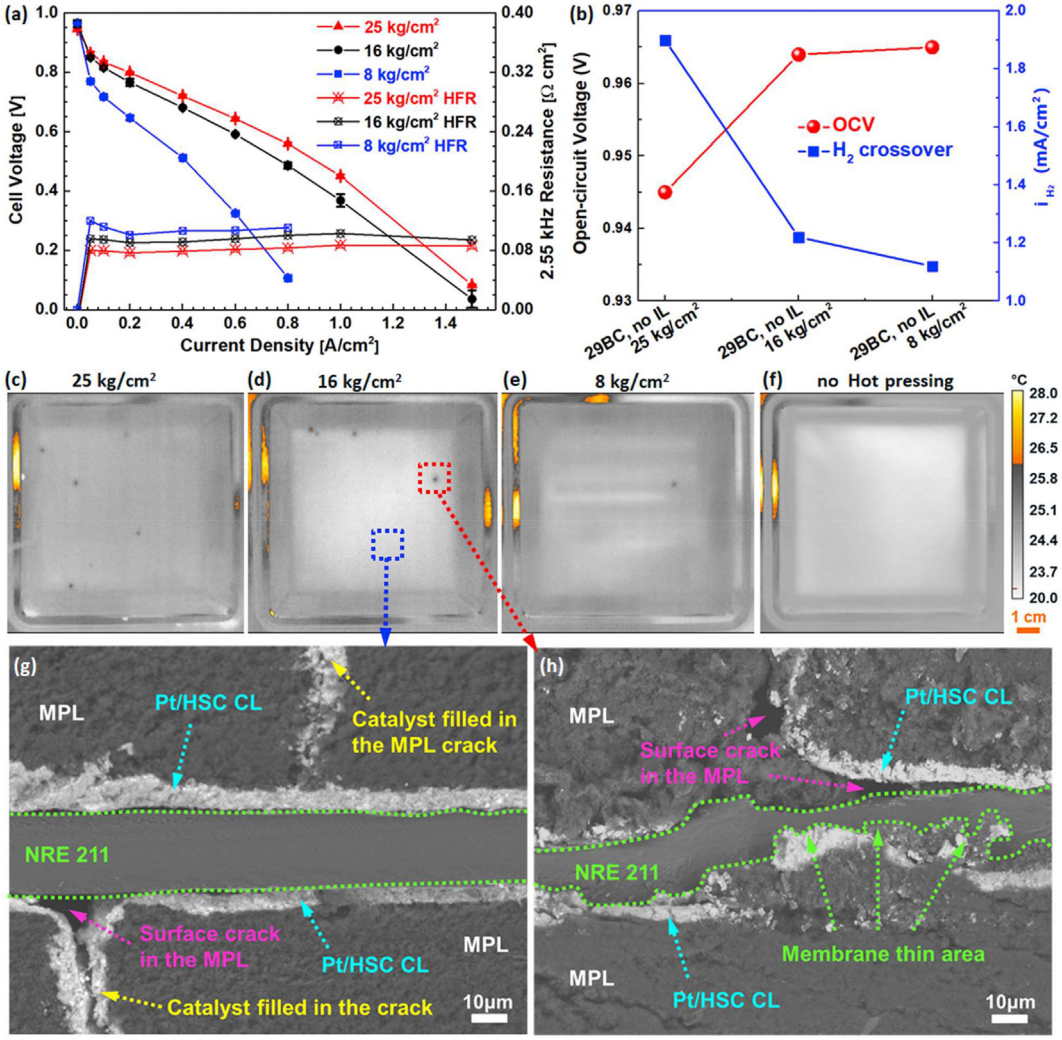

Fig. 2 – Impact of hot pressing compression force on 29BC-based MEAs without ionomer overlayer on: (a) H_2/air polarization and high frequency resistance (HFR); (b) OCV and hydrogen crossover limiting current density (i_{H2}); (c–f) IR thermography of 29BC-based MEAs with different HP compression force and HP temperature of 125 °C. Cross-sectional SEM images of 29BC-based MEAs with 16 kg/cm² HP compression force featuring (g) membrane pristine area with no irregularities and (h) area with a PIM.

performing MEA which fabricated using 25 kg/cm² achieved a voltage of 0.45 V at a current density of 1 A/cm². Our typical performance baseline however is with 0.6 V at 1 A/cm² significantly higher. However, the data clearly show that MEAs with higher HP compression force exhibit better air performance and lower high frequency resistance (HFR). This was also expected, because it is known that hot pressing improves the interfacial contact between the CL and membrane in GDE-based MEAs [32,33]. Fig. 2(b) shows the OCV and the hydrogen crossover limiting current density (i_{H2}) of the same MEAs plotted over the three different HP compression forces. MEAs fabricated at 25 kg/cm² exhibit the lowest OCV of ~0.945 V and the highest i_{H2} of ~1.9 mA/cm². When the HP compression force is decreased, for example to 16 kg/cm², the OCV increased up to ~0.964 V, and the i_{H2} decreased accordingly. The data confirm the correlation of the i_{H2} and the OCV which has been demonstrated and explained in previous work [41]. Additionally, they demonstrate the dependence of both parameters on the HP compression force that was utilized. Fig. 2(c–f) show IR thermography images of the same three hot-pressed cells as well as of an MEA sample that was not hot pressed. The cell with the unpressed MEA was fabricated by assembling two GDEs and a membrane into the hardware and using the same compression torque as for the other three cells. In these images the temperature up to 26.1 °C is displayed in grayscale of increasing intensity, and that above 26.1 °C is displayed in a yellowscale of decreasing intensity. Note that the room temperature (RT) during these measurements was approximately 21 °C and is represented in these images typically by a light grey color. The images in Fig. 2(c–e) reveal discrete local regions that have 1–3 °C increased temperatures, as indicated by the darker grey spots. The quantity of these spots diminishes when lower HP compression forces were used for the MEA fabrication process. At 25 kg/cm² a total of 5 features were detected, while at 16 and 8 kg/cm² only 3 and 1 such features were identified, respectively. No regions

Please cite this article as: Wang M et al., Visualization, understanding, and mitigation of process-induced-membrane irregularities in gas diffusion electrode-based polymer electrolyte membrane fuel cells, International Journal of Hydrogen Energy, https://doi.org/10.1016/j.ijhydene.2021.01.186

with discrete temperature increases were observed when the MEA was not hot pressed, as shown in the image of Fig. 2(f).

Fig. 2(g) shows a SEM cross-section image of an area (blue dashed square) of the sample shown in Fig. 2(d), with no measurable temperature increase. The Nafion 211 membrane is flat and uniform, with a thickness around 20–22 μm. Uniform Pt/HSC catalyst layers with a thickness of ~5 μm are apparent between the membrane and the MPLs. Catalyst material is also observed in the surface cracks of the MPL. This is a side-effect of the spraying process, where the catalyst ink penetrates into the MPL cracks. The lower left region of the image also evidences a gap between the GDE and the membrane at the location of a crack in the MPL. This reduces the CL/membrane contact and may contribute to a reduction in performance as well as provide a site where water can pool, and degradation processes may be promoted.

Fig. 2(h) shows a SEM cross-section image of a selected region with discrete temperature increase, i.e. the region identified by the red dashed square in Fig. 2(d). In contrast to the features of a normal MEA section, as discussed using Fig. 2(g), the morphology of the region with the discrete temperature increase has been strongly impacted. The thickness of the membrane material is not regular in this location. It varies greatly and at the thinnest location the membrane is only about 3–4 μm thick. Thickness variations of the catalyst layer are also apparent. And finally, protruding sections of the GDM are observed, which may have contributed to the significant distortion of the MEA layer structure in this location during the hot press fabrication step. However, the applied hot press process did not seem to have caused any complete penetration of the membrane. This is corroborated by results from our previous study, which indicated that pinholes can lead to localized surface temperatures that are up to 10 °C higher than the surrounding temperature when using the same IR thermography technique [17]. Overall, we can see that the applied hot-press fabrication process led to the creation of what we will refer to as process-induced morphology changes (PIMs). There are many studies focusing on the performance and lifetime impacts of MEA pinholes [42–46], membrane irregularities introduced in the casting process [12,47,48], and membrane degradation [49–54]. However, little understanding exists of MEA-process-induced PIMs, because they are very difficult to detect and their presence goes typically unnoticed. In the course of this study, we investigated more than 10 PIM locations of 29BC-based MEAs that were identified by the IR thermography technique, and always observed this kind of MEA deformation. We are confident that the imaging shown herein is representative. Interestingly, the initial overall performance of the MEAs did not appear to be affected by the quantity of PIMs that are present. For example, the MEA fabricated with 25 kg/cm^2 compression force contained the most PIMs. Its performance, however, was still better than that of the MEAs fabricated with lower HP compression force that contained less PIMs. We therefore conclude, for the cases studied herein, that the initial performance of GDE-based MEAs with PIMs identified by IR thermography is predominantly determined by the quality of the interfacial contact between CL and membrane rather than the state of the membrane after hot pressing.

Fig. 3 shows the results of a similar test series for MEAs fabricated using two different GDM, as specified in the experimental section. The sample set included cathode GDEs with and without thin ionomer overlayers. Fig. 3(a) shows an STEM cross-section at the top surface of the catalyst layer, with additional EDS elemental mapping for platinum (Pt) and fluoride (F) shown in Fig. 3(b),(c). The images indicate a distinguishable ionomer overlayer that was about 150 nm thick and uniformly distributed on top of the catalyst layer. The presence of this overlayer is confirmed by the fluorine-rich top layer in Fig. 3(c) which is clearly separated from the Pt signature of the catalyst layer shown in Fig. 3(b). As indicated by the performance data shown in Fig. 3(d), this thin film dramatically improved the performance of the GDE-based MEAs, regardless of the GDM used. For example, at a current density of 1 A/cm^2 the performance improves from the 0.36 V recorded for the MEAs without ionomer overlayer (magenta and black) to about 0.62 V recorded for the MEAs with overlayer (light blue and dark blue). Note that the ionomer overlayer slightly decreased the HFR of the cells. As discussed in our recent studies on GDE-based MEAs [27,28], this result confirms that the ionomer overlayer facilitates the interfacial proton conduction between catalyst layer and membrane.

Electrochemical hydrogen crossover experiments and IR thermography were performed on these MEAs to assess the impact of the ionomer overlayer on the development of PIMs. Fig. 3(e) shows the OCV and the i_{H2} of the sample set, while Fig. 3(f–g) and (h–i) show IR thermography results of the 29BC- and H23C8-based MEAs, respectively. The data indicate that for both gas diffusion materials, the presence of an ionomer overlayer had no significant effect on the measured OCV, i_{H2}, and the number of detected PIMs. However, the GDM surface smoothness had an effect. At identical HP conditions, the MEAs with a smoother MPL surface, developed fewer measurable PIMs and also displayed higher OCVs.

Taking all the presented data into consideration, the results suggest that, with regards to hot-pressed GDE-based MEAs: (i) The ionomer overlayer is too thin or too compliant to mitigate any deformation that is induced in Nafion 211 during MEA fabrication; (ii) the presence of surface cracks and the overall roughness of the MPL surface directly impact the probability of formation of PIMs during fabrication; and (iii) regardless of how many PIMs exist, the initial performance of all the MEAs that were fabricated with a cathode ionomer overlayer was comparable.

Formation mechanism of membrane irregularities

Fig. 4(a),(b) show top down SEM images onto the MPL and Fig. 4(c),(d) show cross-sectional SEM images through the thickness of the GDM. SGL 29BC material is shown in Fig. 4(a),(c) and Freudenberg H23C8 in Fig. 4(b),(d). In Fig. 4(a) large surface cracks are evident in the MPL of the 29BC sample. In contrast, the MPL surface of the H23C8 shown in Fig. 4(b) appears to be devoid of such surface cracks. The cross-sectional SEM images in Fig. 4(c),(d) show that, while the overall thickness of the two GDMs is very similar, they feature very different MPL thicknesses. The MPL in the H23C8 appears

Please cite this article as: Wang M et al., Visualization, understanding, and mitigation of process-induced-membrane irregularities in gas diffusion electrode-based polymer electrolyte membrane fuel cells, International Journal of Hydrogen Energy, https://doi.org/10.1016/j.ijhydene.2021.01.186

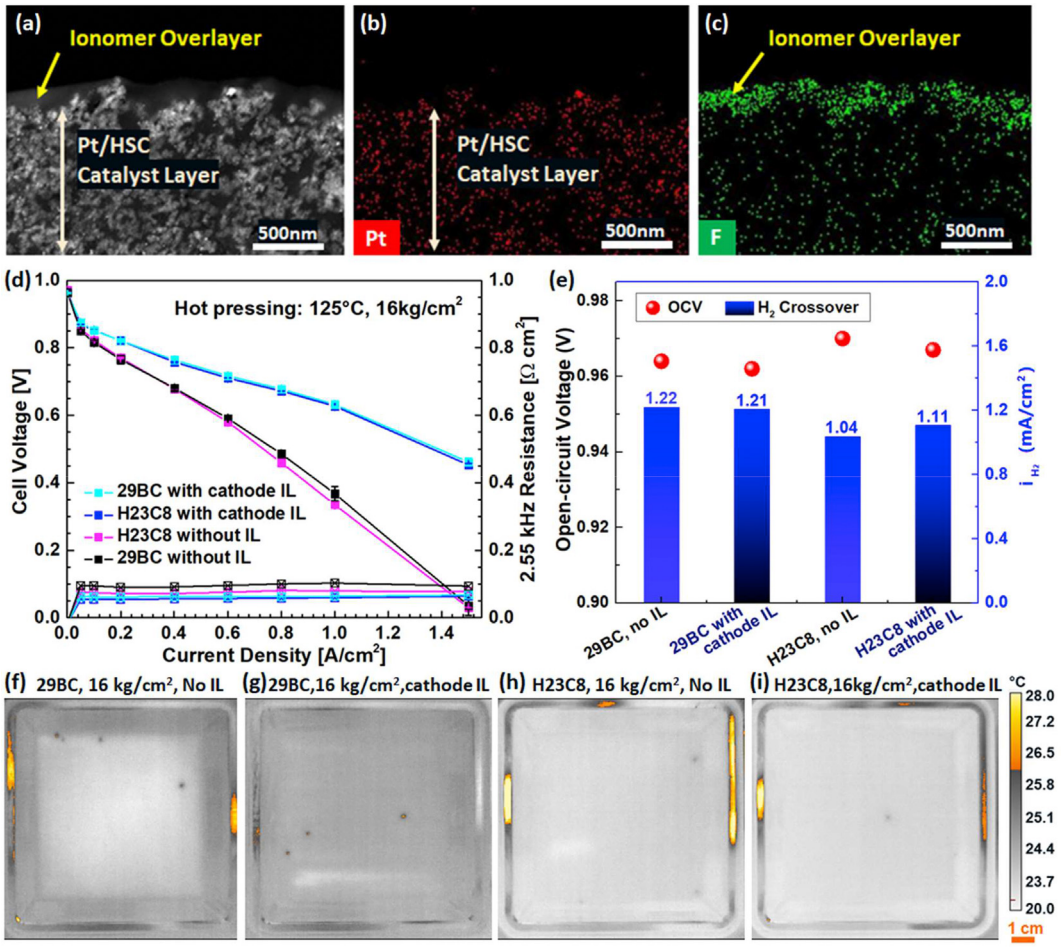

Fig. 3 – STEM images of 29BC-based GDE with 0.023 mg Nafion/cm^2 ionomer overlayer: (a) high-angle annular dark-field (HAADF) image and corresponding elemental mapping of (b) platinum and (c) fluorine. Impact of GDM and presence of ionomer overlayer for MEAs with 16 kg/cm^2 and 125 °C hot-pressing conditions on: (d) H_2/air polarization and high frequency resistance; (e) OCV and hydrogen crossover limiting current density (i_{H2}); (f–i) and IR thermography of GDE-based MEAs with different GDM and ionomer overlayer.

to be less than 30 μm thick, while the MPL thickness in 29BC appears to range from ~80 to 120 μm. Moreover, the carbon fibers in the H23C8 gas diffusion layer appear to be closer to the MPL surface than the fibers in 29BC. Fig. S3 shows the GDL structure of the 29BC and H23C8 materials. The carbon fibers are straight and rigid in 29BC, whereas, in H23C8, the fibers are bent and flexible.

As mentioned earlier, more than 10 PIM locations were investigated for both 29BC-based and H23C8-based MEAs, and similar MEA cross-sectional structures were observed with each diffusion media. Fig. 4(e),(f) exhibit representative cross-sections of 29BC-based and H23C8-based MEAs, respectively, in the vicinity of a PIM location. While Fig. 4(e) does not display the exact location of a membrane distortion as shown in Fig. 2(h), it indicates the presence of some minor membrane deformation and/or thin spots in the vicinity of a surface crack, as previously observed in Figs. 1(a) and 4(a). This suggests that the MPL cracks may create interfacial gaps that allow material to shift during the hot-pressing process, contributing to the formation of membrane irregularities and discontinuous CL/membrane interfaces in the MEA. The image in Fig. 4(f) exhibits the cross-section of a PIM location where a stray fiber points orthogonally in the direction of the membrane. This type of irregularity was predominantly observed in the samples made with H23C8, which may indicate that the thinner MPL and its carbon fiber structure play a significant role in the formation of this irregularity. Overall, there appears to be good contact between the membrane and CLs in both sets of samples, except for the immediate regions at MPL surface cracks.

In summary, our results indicate that the GDM structure impacts the type of membrane irregularities formed during HP. Two phenomena were repeatedly observed during MEA HP. Membrane irregularities forming (i) in the vicinity of MPL surface cracks (see Fig. 4(e), Fig. S4 and Fig. S8), and (ii) at locations where single fibers are oriented orthogonal to the MPL surface and almost penetrate it (see Fig. 4(f) and Fig. S9).

Mitigation of membrane irregularities

GDE-based MEAs with a smoother, less-cracked MPL consistently showed a reduced quantity of PIMs. We now

Please cite this article as: Wang M et al., Visualization, understanding, and mitigation of process-induced-membrane irregularities in gas diffusion electrode-based polymer electrolyte membrane fuel cells, International Journal of Hydrogen Energy, https://doi.org/10.1016/j.ijhydene.2021.01.186

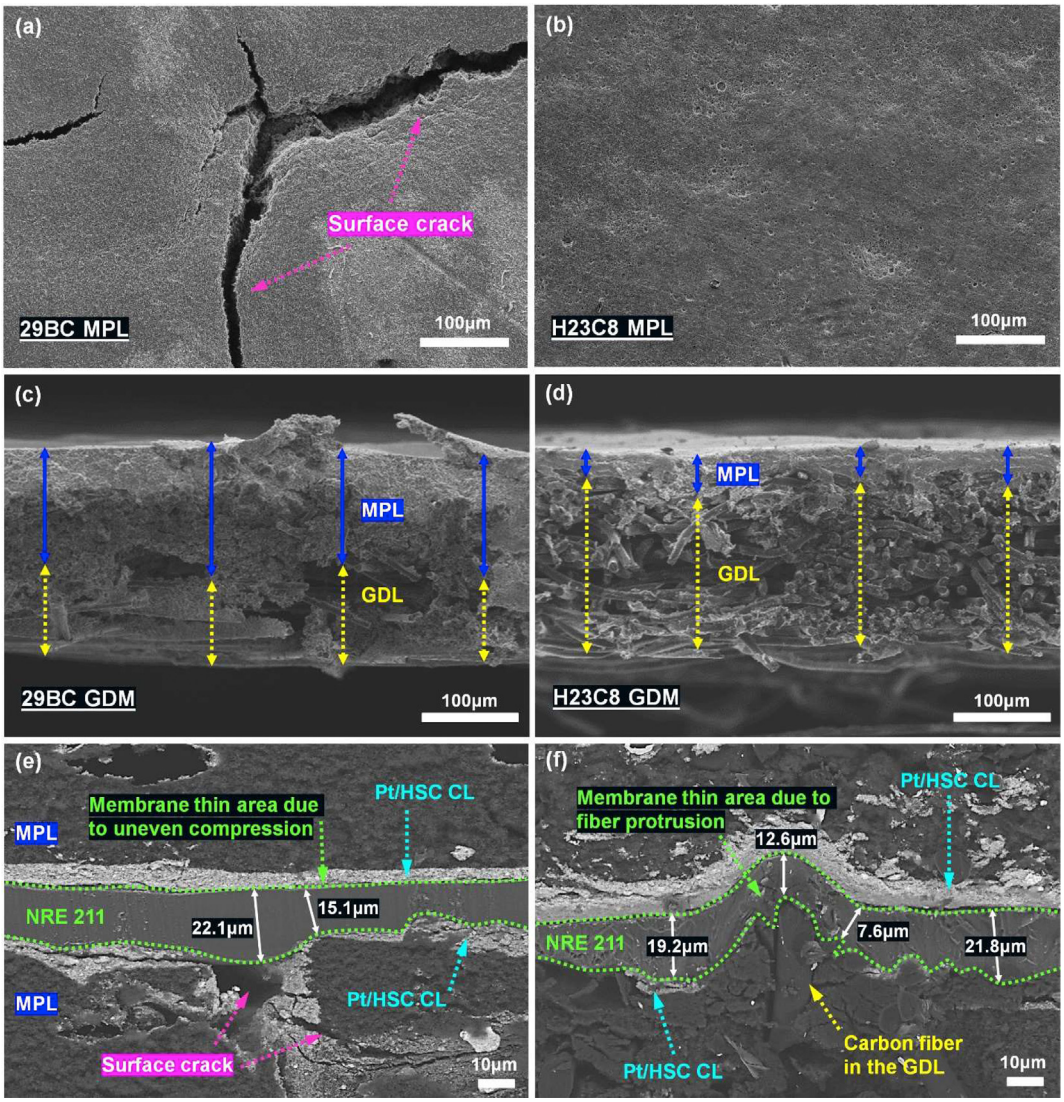

Fig. 4 – Top-down SEM images of the microporous layer of (a) 29BC and (b) H23C8 gas diffusion media; cross-sectional SEM SEI images of (c) 29BC and (d) H23C8 gas diffusion media; cross-sectional SEM BSE images of PIMs in (e) 29BC-based MEA (16 kg/cm^2, 125 °C) and (f) H23C8-based MEA (16 kg/cm^2, 125 °C).

further explore the impact of HP compression force and temperature on the formation of PIMs, selecting H23C8-based MEAs constructed with cathode ionomer overlayers as the study case.

Fig. 5(a–d) show IR thermography results of H23C8-based MEAs fabricated at 125 °C, over a range of HP compression forces from 8 to 25 kg/cm^2. The MEAs shown in Fig. 5(a–c), contain one or two PIMs each, regardless of the compression force that was applied. Apparently, the quantity of PIMs was independent of HP compression force at or above 12 kg/cm^2. However, as shown in Fig. 5(d), when the HP compression force is further reduced to 8 kg/cm^2, a PIM-free pristine MEA was obtained, at least at the sensitivity of the IR method that was used. These data suggest, in conjunction with those shown in Fig. 2(c–f), that the development of PIMs in H23C8-based MEAs may be less sensitive to the HP pressure than that in 29BC-based MEAs. The different nature of the PIMs in these materials, resulting from the differences in MPL surface roughness as well as the presence of orthogonally facing fibers versus cracks, likely plays a significant role in this behavior. Fig. 5(i) additionally shows the OCV and i_{H2} of the H23C8-based MEAs. The MEA hot pressed with 8 kg/cm^2 exhibits the lowest H_2 crossover (0.88 mA/cm^2) and the highest OCV (0.973 V), whereas the other MEAs, fabricated at higher HP compression forces, all had similar i_{H2} and OCVs. These data agree with the observations made using Fig. 2(b–f), and confirm that the number of PIMs impacts the OCV and the i_{H2}.

Fig. 5(e–h) show IR thermography of MEAs fabricated with a compression force of 14 kg/cm^2 and HP temperatures between 110 and 125 °C. Fig. 5(j) shows the OCVs and the i_{H2} of the same MEAs. The data suggest that lowering the HP temperature decreases the likelihood of PIM formation, thus lowering i_{H2} and improving OCV. When decreasing the HP temperature to as low as 110 °C, no PIMs

Please cite this article as: Wang M et al., Visualization, understanding, and mitigation of process-induced-membrane irregularities in gas diffusion electrode-based polymer electrolyte membrane fuel cells, International Journal of Hydrogen Energy, https://doi.org/10.1016/j.ijhydene.2021.01.186

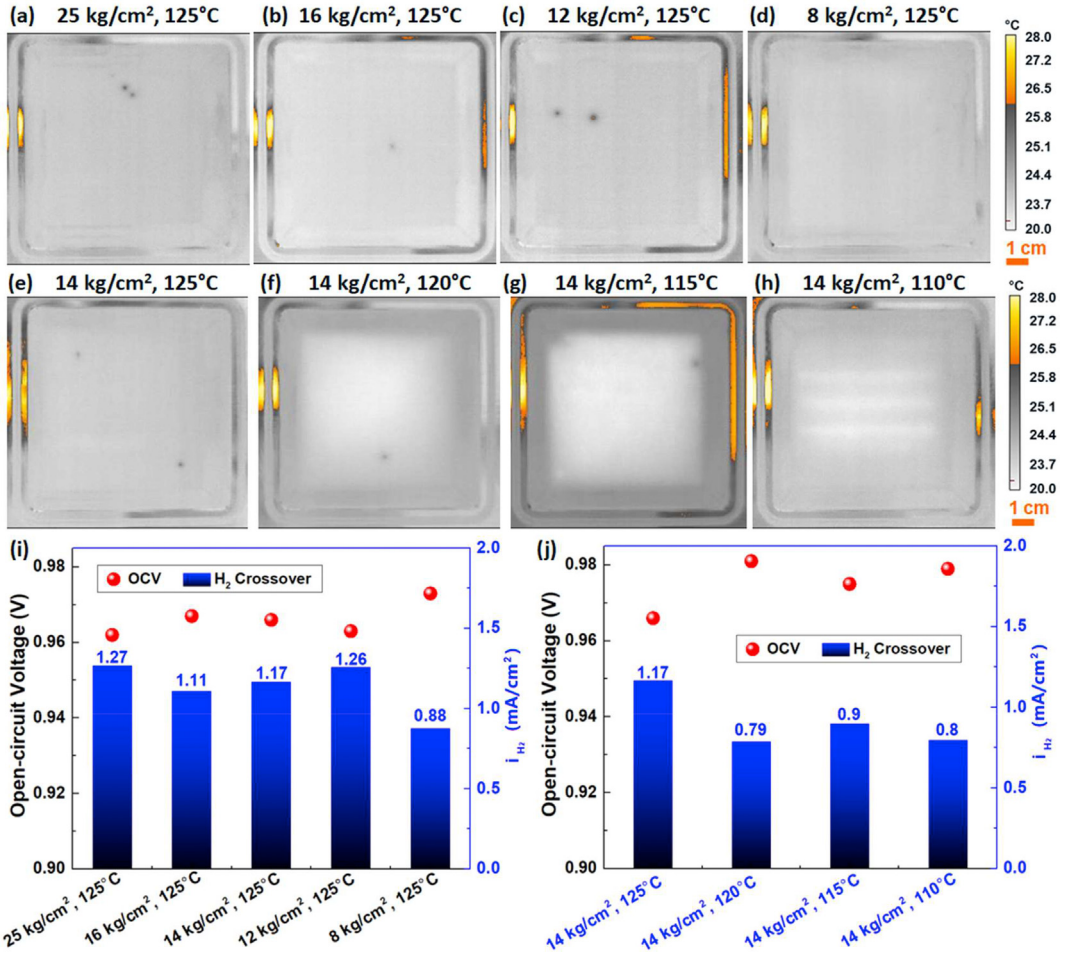

Fig. 5 – IR thermography of H23C8-based MEAs with 0.023 mg Nafion/cm^2 ionomer overlayer hot pressed at (a–d) 125 °C and different compression forces; and (e–h) hot pressed at 14 kg/cm^2 and different temperatures; and their respective (i–j) OCVs and hydrogen crossover limiting current densities.

are detected in the MEA, and the OCV is as high as 0.979 V. These observations likely relate to the first glass transition temperature (T_g) of the Nafion main chain at around 125 °C [55]. The HP temperature has a critical effect on the Nafion membrane because it undergoes macro-structural changes before and after its glass transition, which affects its ability to flow and bond. When lowering the HP temperature below the first Tg, the Nafion membrane exhibits decreased ion mobility and better thermal stability [55–57]. Furthermore, the adhesion at the interface between the membrane and the electrode may be weakened due to the decreased Nafion mobility. PIM formation is also dependent on membrane mobility. Using a HP temperature near the Tg may result in a more fluid membrane environment and promote the development of PIMs. At lower HP temperatures the membrane may have featured a higher structural stability resulting in less electrode/membrane deformations than at a higher HP temperatures. The effect of reducing the HP temperature below 125 °C is apparent for the 120 °C sample, which had the highest OCV and the lowest i_{H2}. Overall, the results imply that careful tuning of the MEA fabrication parameters can be used to successfully mitigate the presence of PIMs.

Impact of hot pressing compression and temperature on initial performance

Fig. 6(a) shows the initial H_2/air performance of MEAs fabricated at 125 °C using HP compression forces ranging from 8 to 25 kg/cm^2. The data indicate that a higher HP compression force results in a lower HFR and a higher initial performance, especially at high current densities (1.0–1.5 A/cm^2). The cell voltage required to provide a current density of 1.5 A/cm^2 ($E^{1.5\ A/cm2}$) of these MEAs ranges from 0.33 V (8 kg/cm^2) to 0.49 V (25 kg/cm^2) (see Fig. 6(c)). The data in Fig. 6(a) thus indicate that a hot-pressing force $\geq$ 12 kg/cm^2 is necessary to maintain a good overall performance and a low HFR. The results imply that fabricating MEAs with a higher HP compression force results in an improved CL/membrane interfacial contact and consequently in a better initial performance.

Fig. 6(b) shows the initial H_2/air performance of MEAs fabricated with 14 kg/cm^2 HP compression force and HP temperatures ranging from 125 to 110 °C. The results indicate that MEAs hot pressed at a higher HP temperature show better mass transport performance and have a lower HFR. As reported by previous studies, the hot-pressing temperature has a critical effect on the perfluorosulfonic acid ionomer, as it

Please cite this article as: Wang M et al., Visualization, understanding, and mitigation of process-induced-membrane irregularities in gas diffusion electrode-based polymer electrolyte membrane fuel cells, International Journal of Hydrogen Energy, https://doi.org/10.1016/j.ijhydene.2021.01.186

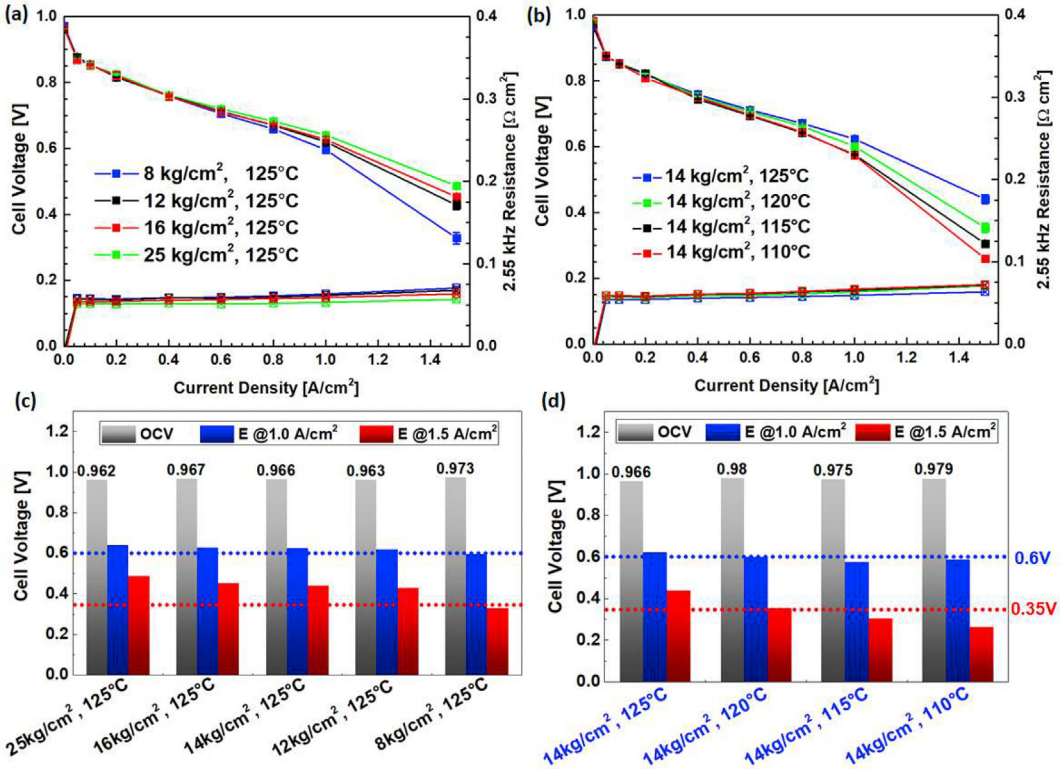

Fig. 6 – Impact of fabrication conditions on performance of H23C8-based MEAs with 0.023 mg Nafion/cm^2 cathode ionomer overlayer: H_2/air polarization curves and high frequency resistance measurements at different hot-pressing (a) compression force and (b) temperature; OCV and cell voltage at 1.0 A/cm^2 and 1.5 A/cm^2 in air polarization curves of MEAs fabricated at different (c) HP compression force and (d) HP temperature compared to expected baselines (dotted lines).

undergoes macro-structural changes before and after its glass transition, affecting its ability to flow and bond [56–59]. When hot pressing the MEA closer to the T_g of Nafion, i.e. 125 °C, the ionomer overlayer and the membrane surface have better fluidity and create an improved interface which decreases the HFR and enhances the performance.

The combined results of Fig. 6(a),(b) suggest that proper HP conditions are required to create a good CL/membrane interface that provides a low HFR and high cell performance. The data indicate that the sensitivity with regards to these parameters is very similar across the ranges the parameters were varied in. Both have a significant effect on the initial performance. We believe that most likely both parameters should be tuned to achieve maximum performance and durability. Fig. 6(c–d) summarizes the performance results (OCV, $E^{1.0\ A/cm2}$, $E^{1.5\ A/cm2}$) of all H23C8-based MEAs. It compares the observed cell voltages to NREL's performance expectations that originate from repeated performance results of NREL's standard research MEA material set, i.e. Nafion® 211, 47% Pt/HSC catalyst at 0.2 mgPt/cm^2 loading on both anode and cathode, and an ionomer:carbon ratio of 0.9. The performance expectations are represented by the dashed red and black lines: i.e. 0.6 V at 1.0 A/cm^2 and 0.35 V at 1.5 A/cm^2, respectively. As previously discussed, the OCV provides good indication as to whether or not PIMs are present in the MEA construct. Comparing the MEAs fabricated with a compression of 14 kg/cm^2 at 125 °C and 120 °C, the higher HP temperature resulted in a reduction of OCV from 0.98 V to 0.966 V, which is directly related to the number of PIMs that were present in the MEA (see Fig. 5(f)), and which resulted in a corresponding increase in i_{H2}. Nonetheless, the performance at high current densities, for example at 1.5 A/cm^2, is better for the MEA fabricated with the hot pressing temperature that was closest to the glass transition temperature of Nafion. Clearly, a trade off exists between creating the desired high initial performance and avoiding the existence of PIMs, the latter being indicated by decreased OCV and increased i_{H2}, and which may act as seed points for MEA degradation and failure, as we shall explore next.

Impact of membrane irregularities on lifetime and failure behavior

Fig. 7(a),(c) shows BOT IR thermography results of two H23C8-based MEA samples fabricated with the following conditions: (a) 25 kg/cm^2, 125 °C; (c) 14 kg/cm^2, 125 °C. Fig. 7(a) shows that the MEA fabricated at HP conditions of 25 kg/cm^2 and 125 °C contains 3 PIMs, whereas Fig. 7(c) shows only 1 PIM in the MEA fabricated with lower HP compression force and temperature. Comparison of Fig. 7(a) and (c) confirm the potential to reduce the number of PIMs by modifying the MEA fabrication conditions.

Subsequent to the BOT IR thermography, the MEAs were exposed to the described AST. When the OCV of a MEA reached a value of 0.9 V or lower, the AST was stopped, and the EOT IR thermography data was taken. Fig. 7(b),(d) show the

Please cite this article as: Wang M et al., Visualization, understanding, and mitigation of process-induced-membrane irregularities in gas diffusion electrode-based polymer electrolyte membrane fuel cells, International Journal of Hydrogen Energy, https://doi.org/10.1016/j.ijhydene.2021.01.186

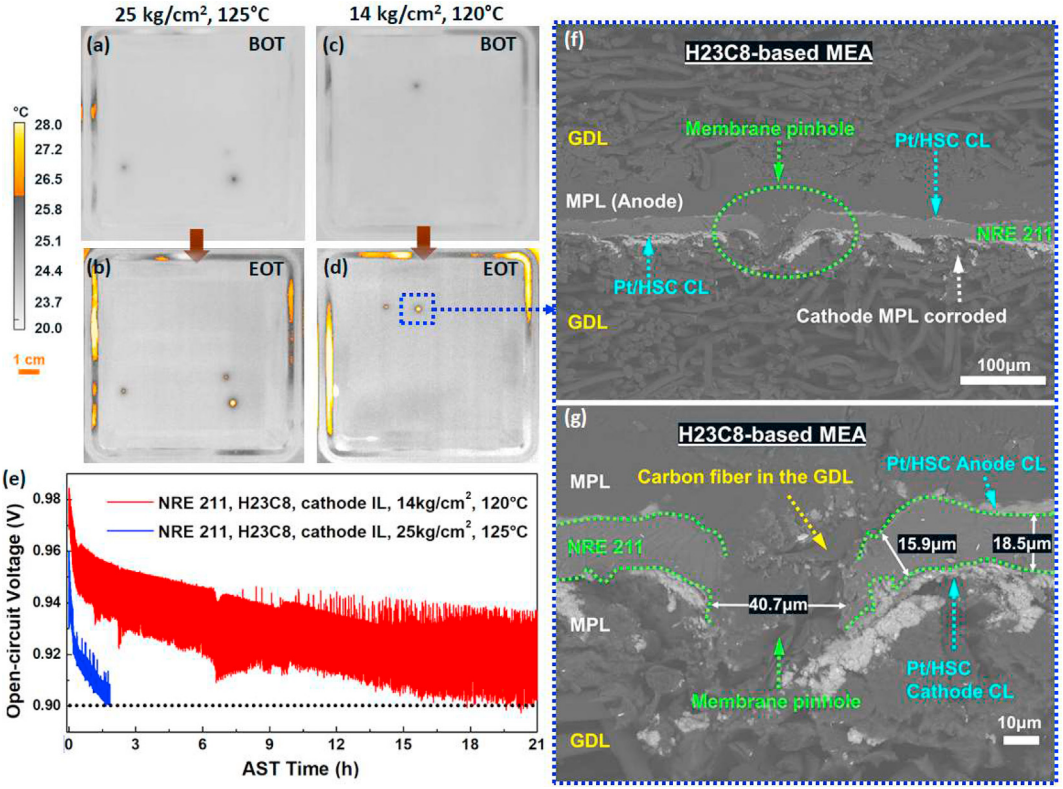

Fig. 7 – IR thermography of H23C8-based MEA (25 kg/cm², 125 °C) at (a) BOT and (b) EOT; IR thermography of H23C8-based MEA (14 kg/cm², 120 °C) at (c) BOT and (d) EOT; (e). OCV decay profile of H23C8-based MEA (25 kg/cm², 125 °C) and H23C8-based MEA (14 kg/cm², 120 °C) during AST operation; (f, g). Cross-sectional SEM BSE images of failure point of H23C8-based MEA (14 kg/cm², 120 °C) at EOT under different magnifications.

results of the EOT IR thermography, using the same sample order from above. Several of the PIMs observed at BOT developed during the AST operation into locations of significantly increased hydrogen crossover. Such locations are indicated by the spots of orange color in the EOT results shown in Fig. 7(b),(d). The orange color indicates a temperature increase of ~7 °C at this location, which, based on our prior work, enables us to classify them as failure points of the membrane. The correlation of the location of detected PIMs at BOT and that of failure points at EOT allows us to conclude that these PIMs act as seed points for failure in fuel cells. Furthermore, the presence of additional failure points not identified in the BOT IR thermography, e.g. the one to the left of the blue dotted box in Fig. 7(d), may indicate that (i) our method is not sensitive enough to detect all PIMs prior to operation and/or (ii) some failure points have developed via other mechanisms, at locations where PIMs were not initially present.

Fig. 7(e) shows the OCV decay profile vs. time of the MEA samples during the course of the AST, i.e. after the BOT IR Thermography and before the EOT. The H23C8-based MEA that was fabricated with adjusted HP conditions (14 kg/cm², 120 °C) had much longer lifetime than the other MEA. These results suggest that the number of PIMs shortens the AST lifetime of the MEAs. It further indicates that the AST lifetime of a H23C8-based MEA can be extended from 1.6 h to about 21 h, i.e. by a factor of about 13, by adjusting the HP conditions and reducing the initial count of PIMs. Such learnings are especially significant within the context of heavy-duty fuel cell applications, such as long-haul trucks, where the target lifetime of the stack is 5x longer than that for light-duty vehicles.

One failure point of the MEA with adjusted HP conditions was further investigated. Fig. 7(f),(g) show BSE SEM images of the MEA cross-section around this failure point – identified by the blue dotted square in Fig. 7(d) – using two different magnifications. The images reveal that the membrane layer, which can be seen between the two brighter Pt/HSC catalyst layers, was discontinuous, and that a pinhole developed. Fig. 7(g) shows this location with higher magnification. The failure point consisted of a ~40 μm diameter membrane pinhole at a location where a carbon fiber protruded from the H23C8 GDM.

It should be noted that the phenomena of failure point development is not dependent on the gas diffusion media. We also investigated 29BC-based MEA and observed that PIMs developed into pinholes, as shown in Fig. S11. The IR images in Fig. S11 (a),(c) show that the 29BC-based MEA contained 7 PIMs, whereas the H23C8-based MEA, both hot-pressed at the same conditions, contained 3 PIMs. This agrees with our prior observation that the fabrication conditions are not the only variable contributing to the development of PIMs, but that the substrate material used also plays an important role. Moreover, according to Fig. S11 (b),(d), regardless of the gas

Please cite this article as: Wang M et al., Visualization, understanding, and mitigation of process-induced-membrane irregularities in gas diffusion electrode-based polymer electrolyte membrane fuel cells, International Journal of Hydrogen Energy, https://doi.org/10.1016/j.ijhydene.2021.01.186

diffusion media, the initial PIMs eventually developed into failure points. Fig. S11 (e) also shows that the MEA with a higher number of PIMs had a shorter lifetime, in good agreement with the discussion above.

Conclusion

Process-induced membrane irregularities were detected and localized using NREL's quasi-in-situ IR thermography subsequent to the fabrication of GDE-based MEAs. The structure and formation mechanism of these membrane irregularities were further studied in a large number of samples by cross-sectional SEM. Irregularities were observed to form near MPL surface cracks due to uneven compression and membrane deformation and at locations of GDL fiber penetration into the membrane. The effect of fabrication conditions such as addition of ionomer overlayer, MPL roughness, and hot pressing compression force and temperature on membrane irregularity development, hydrogen crossover, HFR and initial cell performance were systematically investigated. The addition of ionomer overlayer exhibited negligible effect on the amount of membrane irregularities, but, consistent with our prior studies, dramatically improved the performance by facilitating the interfacial proton conduction between CL and membrane. Under the same hot-pressing condition, MEAs fabricated using GDM with a rougher MPL surface exhibited a higher amount of PIMs. MEAs processed with more aggressive hot-pressing conditions (higher compression force and/or HP temperature) were observed to have a higher number of membrane irregularities, higher hydrogen crossover and lower open-circurt voltage. Despite this, these MEAs displayed increased initial performance and decreased HFR due to better contact between CL and membrane. Under accelerated testing, however, membrane irregularities were demonstrated to be seed points for failure, and to shorten MEA lifetime dramatically. We thus identify, at least within the scope of this study, a conundrum: higher initial performance, or longer lifetime? We have clearly shown that, in the case of prioritization of the latter, the selection of specific GDM properties and HP fabrication conditions generally enabled the mitigation of PIMs and extended AST lifetime. Certainly, further study is warranted, especially given the extensive and important new focus on heavy-duty fuel cell applications, for which durability and extended lifetime are tantamount. We further note that, while the effect of GDM morphology and structure was explored herein, the impact of membrane thickness and architecture, i.e. with and without reinforcement, on PIM formation is clearly of interest, and is the topic of a follow-on study.

Associated content

List of contents in Appendix A. Supplementary Data: configuration of a 50 cm^2 GDE-based MEA with edge protection; experiment setup of quasi-in-situ IR thermography for spatial hydrogen crossover visualization; optical miscopy images of the MPL and GDL of the two different gas diffusion media, H23C8 and 29BC; cross-sectional SEM BSE images of the membrane irregularity area shown in Fig. 2(g) at a lower magnification; cross-sectional SEM SEI and BSE images of the membrane irregularity area shown in Fig. 4(b); H_2 LSVs of 29BC- and H23C8-based MEAs fabricated at different hot-pressing conditions; cross-sectional SEM BSE images of multiple membrane irregularities of 29BC-based and H23C8-based MEA fabricated at 125 °C and 16 kg/cm^2; cross-sectional SEM SEI image of the failure point of H23C8-based MEA (14 kg/cm^2, 120 °C) at EOT shown in Fig. 7(i).

Declaration of competing interest

The authors declare that they have no known competing financial interests or personal relationships that could have appeared to influence the work reported in this paper.

Acknowledgment

This work was authored in part by the National Renewable Energy Laboratory, operated by Alliance for Sustainable Energy, LLC, for the U.S. Department of Energy (DOE) under Contract No. DE-AC36-08GO28308. Funding provided by the U.S. Department of Energy Office of Energy Efficiency and Renewable Energy Hydrogen and Fuel Cell Technologies Office (HFTO), Technology Manager Nancy Garland. The U.S. Government retains and the publisher, by accepting the article for publication, acknowledges that the U.S. Government retains a nonexclusive, paid-up, irrevocable, worldwide license to publish or reproduce the published form of this work, or allow others to do so, for U.S. Government purposes. The views expressed in the article do not necessarily represent the views of the DOE or the U.S. Government.

Appendix A. Supplementary data

Supplementary data to this article can be found online at https://doi.org/10.1016/j.ijhydene.2021.01.186.

REFERENCES

[1] Thompson ST, James BD, Huya-Kouadio JM, Houchins C, DeSantis DA, Ahluwalia R, Wilson AR, Kleen G, Papageorgopoulos D. Direct hydrogen fuel cell electric vehicle cost analysis: system and high-volume manufacturing description, validation, and outlook. J Power Sources 2018;399:304–13.
[2] O'Hayre R, Cha S-W, Colella W, Prinz FB. Fuel cell fundamentals. 2016. https://doi.org/10.1002/9781119191766. ISBN: 978-1-119-11380-5.
[3] Veziroglu A, Macario R. Fuel cell vehicles: state of the art with economic and environmental concerns. Int J Hydrogen Energy 2011;36:25–43.
[4] Boscaino V, Miceli R, Capponi G, Ricco Galluzzo G. A review of fuel cell based hybrid power supply architectures and algorithms for household appliances. Int J Hydrogen Energy 2014;39:1195–209.

[5] Dodds PE, Staffell I, Hawkes AD, Li F, Grünewald P, McDowall W, Ekins P. Hydrogen and fuel cell technologies for heating: a review. Int J Hydrogen Energy 2015;40:2065–83.
[6] Omrani R, Shabani B. Gas diffusion layer modifications and treatments for improving the performance of proton exchange membrane fuel cells and electrolysers: a review. Int J Hydrogen Energy 2017;42:28515–36.
[7] Othman R, Dicks AL, Zhu Z. Non precious metal catalysts for the PEM fuel cell cathode. Int J Hydrogen Energy 2012;37:357–72.
[8] Sadhasivam T, Dhanabalan K, Roh S-H, Kim T-H, Park K-W, Jung S, Kurkuri MD, Jung H-Y. A comprehensive review on unitized regenerative fuel cells: crucial challenges and developments. Int J Hydrogen Energy 2017;42:4415–33.
[9] Zhang S, Yuan X, Wang H, Merida W, Zhu H, Shen J, Wu S, Zhang J. A review of accelerated stress tests of MEA durability in PEM fuel cells. Int J Hydrogen Energy 2009;34:388–404.
[10] Mauger SA, Neyerlin KC, Yang-Neyerlin AC, More KL, Ulsh M. Gravure coating for Roll-to-Roll manufacturing of Proton-Exchange-Membrane fuel cell catalyst layers. J Electrochem Soc 2018;165:F1012–8.
[11] Ulsh M, Sopori B, Aieta NV, Bender G. Challenges to high-volume production of fuel cell materials: quality control. ECS Trans 2013;50:919–26.
[12] Phillips A, Ulsh M, Mackay J, Harris T, Shrivastava N, Chatterjee A, Porter J, Bender G. The effect of membrane casting irregularities on initial fuel cell performance. Fuel Cell 2020;20:60–9.
[13] Phillips A, Ulsh M, Neyerlin KC, Porter J, Bender G. Impacts of electrode coating irregularities on polymer electrolyte membrane fuel cell lifetime using quasi in-situ infrared thermography and accelerated stress testing. Int J Hydrogen Energy 2018;43:6390–9.
[14] Phillips A, Ulsh M, Porter J, Bender G. Utilizing a segmented fuel cell to study the effects of electrode coating irregularities on PEM fuel cell initial performance. Fuel Cell 2017;17:288–98.
[15] Bender G, Felt W, Ulsh M. Detecting and localizing failure points in proton exchange membrane fuel cells using IR thermography. J Power Sources 2014;253:224–9.
[16] Ulsh M, Porter JM, Bittinat DC, Bender G. Defect detection in fuel cell gas diffusion electrodes using infrared thermography. Fuel Cell 2016;16:170–8.
[17] Ulsh M, DeBari A, Berliner JM, Zenyuk IV, Rupnowski P, Matvichuk L, Weber AZ, Bender G. The development of a through-plane reactive excitation technique for detection of pinholes in membrane-containing MEA sub-assemblies. Int J Hydrogen Energy 2019;44:8533–47.
[18] Das PK, Weber AZ, Bender G, Manak A, Bittinat D, Herring AM, Ulsh M. Rapid detection of defects in fuel-cell electrodes using infrared reactive-flow-through technique. J Power Sources 2014;261:401–11.
[19] Bittinat DC, Bender G, Porter JM, Ulsh M. Defect detection in fuel cell gas diffusion electrodes using infrared thermography. ECS Trans 2013;58:495–503.
[20] Zenyuk IV, Englund N, Bender G, Weber AZ, Ulsh M. Reactive impinging-flow technique for polymer-electrolyte-fuel-cell electrode-defect detection. J Power Sources 2016;332:372–82.
[21] Aieta NV, Das PK, Perdue A, Bender G, Herring AM, Weber AZ, Ulsh MJ. Applying infrared thermography as a quality-control tool for the rapid detection of polymer-electrolyte-membrane-fuel-cell catalyst-layer-thickness variations. J Power Sources 2012;211:4–11.
[22] Lee DY, Elgowainy A, Kotz A, Vijayagopal R, Marcinkoski J. Life-cycle implications of hydrogen fuel cell electric vehicle technology for medium- and heavy-duty trucks. J Power Sources 2018;393:217–29.
[23] Marcinkoski J, Vijayagopal R, Adams J, James B, Kopasz J, Ahluwalia R. Hydrogen class 8 long haul truck targets. Subsection of the electrified powertrain roadmap. Technical targets for hydrogen-fueled long-haul tractor-trailer trucks. Adv. Truck Technol 2019. DOE.
[24] Mehta V, Cooper JS. Review and analysis of PEM fuel cell design and manufacturing. J Power Sources 2003;114:32–53.
[25] Lin J-C, Lai C-M, Ting F-P, Chyou S-D, Hsueh K-L. Influence of hot-pressing temperature on the performance of PEMFC and catalytic activity. J Appl Electrochem 2009;39:1067–73.
[26] Shahgaldi S, Alaefour I, Li X. Impact of manufacturing processes on proton exchange membrane fuel cell performance. Appl Energy 2018;225:1022–32.
[27] Mauger SA, Pfeilsticker JR, Wang M, Medina S, Yang-Neyerlin AC, Neyerlin KC, Stetson C, Pylypenko S, Ulsh M. Fabrication of high-performance gas-diffusion-electrode based membrane-electrode assemblies. J Power Sources 2020;450:227581.
[28] Wang M, Medina S, Pfeilsticker JR, Pylypenko S, Ulsh M, Mauger SA. Impact of microporous layer roughness on gas-diffusion-electrode-based polymer electrolyte membrane fuel cell performance. ACS Appl Energy Mater 2019;2:7757–61.
[29] Andersen SM, Dhiman R, Larsen MJ, Skou E. Importance of electrode hot-pressing conditions for the catalyst performance of proton exchange membrane fuel cells. Appl. Catal. B Environ. al 2015;172–173:82–90.
[30] Sassin MB, Garsany Y, Gould BD, Swider-Lyons KE. Fabrication method for laboratory-scale high-performance membrane electrode assemblies for fuel cells. Anal Chem 2017;89:511–8.
[31] Suzuki T, Tanaka H, Hayase M, Tsushima S, Hirai S. Investigation of porous structure formation of catalyst layers for proton exchange membrane fuel cells and their effect on cell performance. Int J Hydrogen Energy 2016;41:20326–35.
[32] Okur O, Karadag Çİ, San FGB, Okumuş E, Behmenyar G. Optimization of parameters for hot-pressing manufacture of membrane electrode assembly for PEM (polymer electrolyte membrane fuel cells) fuel cell. Energy 2013;57:574–80.
[33] Therdthianwong A, Manomayidthikarn P, Therdthianwong S. Investigation of membrane electrode assembly (MEA) hot-pressing parameters for proton exchange membrane fuel cell. Energy 2007;32:2401–11.
[34] Wang M, Park JH, Kabir S, Neyerlin KC, Kariuki NN, Lv H, Stamenkovic VR, Myers DJ, Ulsh M, Mauger SA. Impact of catalyst ink dispersing methodology on fuel cell performance using in-situ X-ray scattering. ACS Appl Energy Mater 2019;2:6417–27.
[35] Van Cleve T, Khandavalli S, Chowdhury A, Medina S, Pylypenko S, Wang M, More KL, Kariuki N, Myers DJ, Weber AZ, Mauger SA, Ulsh M, Neyerlin KC. Dictating Pt-based electrocatalyst performance in polymer electrolyte fuel cells, from formulation to application. ACS Appl Mater Interfaces 2019;11:46953–64.
[36] Wang M, Rome G, Phillips A, Ulsh M, Bender G. Effective electrode edge protection for proton exchange membrane fuel cell drive cycle operation. ECS Trans 2019;92:351–9.
[37] Kabir S, Myers DJ, Kariuki N, Park J, Wang G, Baker A, Macauley N, Mukundan R, More KL, Neyerlin KC. Elucidating the dynamic nature of fuel cell electrodes as a function of conditioning: an ex situ material characterization and in situ electrochemical diagnostic study. ACS Appl Mater Interfaces 2019;11:45016–30.
[38] Zhang J, Paine L. Methods and processes to recover voltage loss of pem fuel cell stack. US Appl; 2011.
[39] Lai Y-H, Rahmoeller KM, Hurst JH, Kukreja RS, Atwan M, Maslyn AJ, Gittleman CS. Accelerated stress testing of fuel

Please cite this article as: Wang M et al., Visualization, understanding, and mitigation of process-induced-membrane irregularities in gas diffusion electrode-based polymer electrolyte membrane fuel cells, International Journal of Hydrogen Energy, https://doi.org/10.1016/j.ijhydene.2021.01.186

cell membranes subjected to combined mechanical/chemical stressors and cerium migration. J Electrochem Soc 2018;165:F3217–29.
[40] Neyerlin KC, Gu W, Jorne J, Gasteiger HA. Determination of catalyst unique parameters for the oxygen reduction reaction in a PEMFC. J Electrochem Soc 2006;153:A1955–63.
[41] Vilekar SA, Datta R. The effect of hydrogen crossover on open-circuit voltage in polymer electrolyte membrane fuel cells. J Power Sources 2010;195:2241–7.
[42] Bodner M, Hochenauer C, Hacker V. Effect of pinhole location on degradation in polymer electrolyte fuel cells. J Power Sources 2015;295:336–48.
[43] Kusoglu A, Weber AZ. A mechanistic model for pinhole growth in fuel cell membranes during cyclic loads. J Electrochem Soc 2014;161:E3311–22.
[44] Huang BT, Chatillon Y, Bonnet C, Lapicque F, Leclerc S, Hinaje M, Raël S. Experimental investigation of pinhole effect on MEA/cell aging in PEMFC. Int J Hydrogen Energy 2013;38:543–50.
[45] Reshetenko TV, Bender G, Bethune K, Rocheleau R. Application of a segmented cell setup to detect pinhole and catalyst loading defects in proton exchange membrane fuel cells. Electrochim Acta 2012;76:16–25.
[46] Lü W, Liu Z, Wang C, Mao Z, Zhang M. The effects of pinholes on proton exchange membrane fuel cell performance. Int J Energy Res 2011;35:24–30.
[47] Moukheiber E, Bas C, Flandin L. Understanding the formation of pinholes in PFSA membranes with the essential work of fracture (EWF). Int J Hydrogen Energy 2014;39:2717–23.
[48] Bhamidipati KL, Didari S, Bedell P, Harris TAL. Wetting phenomena during processing of high-viscosity shear-thinning fluid. J. Nonnewton. Fluid Mech. 2011;166:723–33.
[49] De Moor G, Bas C, Charvin N, Dillet J, Maranzana G, Lottin O, Caque N, Rossinot E, Flandin L. Perfluorosulfonic acid membrane degradation in the hydrogen inlet region: a macroscopic approach. Int J Hydrogen Energy 2016;41:483–96.
[50] Lim C, Ghassemzadeh L, Van Hove F, Lauritzen M, Kolodziej J, Wang GG, Holdcroft S, Kjeang E. Membrane degradation during combined chemical and mechanical accelerated stress testing of polymer electrolyte fuel cells. J Power Sources 2014;257:102–10.
[51] Kreitmeier S, Schuler GA, Wokaun A, Büchi FN. Investigation of membrane degradation in polymer electrolyte fuel cells using local gas permeation analysis. J Power Sources 2012;212:139–47.
[52] De Moor G, Bas C, Charvin N, Moukheiber E, Niepceron F, Breilly N, Andre J, Rossinot E, Claude E, Alberola ND, Flandin L. Understanding membrane failure in PEMFC: comparison of diagnostic tools at different observation scales. Fuel Cell 2012;12:356–64.
[53] Borup R, Meyers J, Pivovar B, Kim YS, Mukundan R, Garland N, Myers D, Wilson M, Garzon F, Wood D, Zelenay P, More K, Stroh K, Zawodzinski T, Boncella J, McGrath JE, Inaba M, Miyatake K, Hori M, Ota K, Ogumi Z, Miyata S, Nishikata A, Siroma Z, Uchimoto Y, Yasuda K, Kimijima K, Iwashita N. Scientific aspects of polymer electrolytefuel cell durability and degradation. Chem Rev 2007;107:3904–51.
[54] Li Y, Dillard DA, Case SW, Ellis MW, Lai Y-H, Gittleman CS, Miller DP. Fatigue and creep to leak tests of proton exchange membranes using pressure-loaded blisters. J Power Sources 2009;194:873–9.
[55] Jung H-Y, Kim JW. Role of the glass transition temperature of Nafion 117 membrane in the preparation of the membrane electrode assembly in a direct methanol fuel cell (DMFC). Int J Hydrogen Energy 2012;37:12580–5.
[56] DeBonis D, Mayer M, Omosebi A, Besser RS. Analysis of mechanism of Nafion® conductivity change due to hot pressing treatment. Renew Energy 2016;89:200–6.
[57] Martemianov S, Raileanu Ilie VA, Coutanceau C. Improvement of the proton exchange membrane fuel cell performances by optimization of the hot pressing process for membrane electrode assembly. J Solid State Electrochem 2014;18:1261–9.
[58] Osborn SJ, Hassan MK, Divoux GM, Rhoades DW, Mauritz KA, Moore RB. Glass transition temperature of perfluorosulfonic acid ionomers. Macromolecules 2007;40:3886–90.
[59] Yu S, Jung D. Thermal management strategy for a proton exchange membrane fuel cell system with a large active cell area. Renew Energy 2008;33:2540–8.

Please cite this article as: Wang M et al., Visualization, understanding, and mitigation of process-induced-membrane irregularities in gas diffusion electrode-based polymer electrolyte membrane fuel cells, International Journal of Hydrogen Energy, https://doi.org/10.1016/j.ijhydene.2021.01.186